Dynamics and control of a quasi-one-dimensional spin system

P. Cappellaro,[1] C. Ramanathan,[2] and D. G. Cory[2]
[1]*ITAMP, Harvard-Smithsonian Center for Astrophysics, Cambridge, Massachusetts 02138, USA*
[2]*Department of Nuclear Science and Engineering, Massachusetts Institute of Technology, Cambridge, Massachusetts 02139, USA*
(Received 7 June 2007; published 18 September 2007)

We study experimentally a system comprised of linear chains of spin-1/2 nuclei that provides a test bed for multibody dynamics and quantum-information processing. This system is a paradigm for a class of quantum-information processing devices that can perform particular tasks even without universal control of the whole quantum system. We investigate the extent of control achievable on the system with current experimental apparatus and methods to gain information on the system state, when full tomography is not possible and in any case highly inefficient.

DOI: 10.1103/PhysRevA.76.032317 PACS number(s): 03.67.Hk, 03.67.Lx, 76.90.+d

I. INTRODUCTION

The dynamics and control of complex quantum many-body systems has elicited renewed interest within the field of quantum-information science. Not only is there a need to improve coherent control of an increasing number of qubits to build a scalable quantum computer, but also new task-oriented devices (such as quantum-information transport, quantum cloning and simulation devices) constitute a new paradigm for quantum-information processing (QIP), in which even a partial control over the system is enough to accomplish the desired task. Of course, even for these devices a precise knowledge of their dynamics is an indispensable ingredient, thus spurring new investigations and the development of new tools for coherent control.

Here we study a physical system that presents a simpler quantum dynamics because of its one-dimensional (1D) geometry, while still retaining the full complexity of many-body dynamics. The system is a single crystal of fluorapatite (FAp), where we focus on the spin degrees of freedom of the fluorine-19 nuclei. This spin system has already been studied in the nuclear magnetic resonance (NMR) literature and proposed for quantum computation.

The goals of this study are to investigate the extent of our control of the system when the control Hamiltonians can only act collectively on all the spins and to devise methods for extracting information from the system when state tomography is not only inefficient, but also impossible because we can only detect the collective magnetization. We do not consider here issues of decoherence mechanisms and rates, relying on the long coherence times of nuclear spins for performing all experiments in the coherent regime. Decoherence properties of quantum many-body systems are, however, a very important area of study [1–3], and preliminary results regarding the system under investigation have already been presented [4].

In Sec. II we first show how we can push the limits of our control when preparing a particular initial state, which is of interest for some tasks such as quantum-information transfer and quantum simulations [5]. Starting from the thermal equilibrium state, we will show how to create a state where only the two spins at the ends of the chain are polarized, while all other spins are in the identity state. Also, this state is a first step toward showing universal control of the system, as it has been proved that collective control of a qubit chain plus control of the spins at the chain ends is enough for universal control of the system [6,7]. In Sec. III we present the characteristics of the physical system and the experimental apparatus as well as the first indications that we successfully prepared the desired state. We then explain in Sec. IV how we can extract enough information from the detection of the collective magnetization to verify the creation of this desired initial state. The measurement is preceded by evolution under a propagator engineered to let emerge the many-body properties of the system. We use the technique of multiple quantum coherence (MQC) [8] as a way to perform a partial tomography of the system and gain further information on its state. In particular, we take advantage of the lower dimensionality of the system, which makes possible an analytical description of the evolution. We finally present experimental results in good agreement with the theoretical predictions, thus proving the preparation of the desired state.

II. SELECTING THE SPINS AT THE EXTREMITIES OF THE LINEAR CHAIN

There has been recently a remarkable interest in linear chains of spins [9–13], as well as their simulation through atomic lattices [14]. The physical system we are interested in (a crystal of fluorapatite) can be modeled by a linear chain of spin-1/2 particles of a size ($N \gtrsim 10$) such that many-body properties emerge. The system is put at room temperature in a large magnetic field and is addressed through radio-frequency (rf) pulses. The internal Hamiltonian of the system in a frame rotating at the larmor frequency is given by the secular part of the dipolar Hamiltonian

$$\mathcal{H}_{\mathrm{dip}} = \sum_{ij} b_{ij} \left[\sigma_z^i \sigma_z^j - \frac{1}{2}(\sigma_x^i \sigma_x^j + \sigma_y^i \sigma_y^j) \right], \tag{1}$$

while external control is provided by the rf Hamiltonian

$$\mathcal{H}_{\mathrm{rf}} = \omega_{\mathrm{rf}}(t) \sum_i \left[\sigma_x^i \cos \phi(t) + \sigma_y^i \sin \phi(t) \right]. \tag{2}$$

The control is therefore collective; that is, we can only address all the spins in the chain together: This limitation

precludes universal control on the system. A recent scheme for QIP [6,7] showed, however, that adding to the collective control the ability to manipulate the spins at the chain ends enables universal quantum computation. A step toward achieving universal control would be to demonstrate at least a partial addressability of an individual spin. To prove the extent of our control of the system, we set up to prepare a particular quantum state, in which only the spins at the extremities of the chain are polarized: $\rho_0=\mathbb{1}+\epsilon(\sigma_z^1+\sigma_z^N)$ (notice that this highly mixed state emerges from an ensemble average over many chains that are here considered as independent and equivalent systems). This state not only proves that we can break the internal symmetry of the system, but is also a useful state, for example, for quantum-information transport [15].

The spins at the extremities of the chain only have one nearest neighbor to which they are strongly coupled. This implies a different dynamics under the internal dipolar Hamiltonian with respect to the other spins. Taking advantage of this fact and complementing unitary control with incoherent control [16] will allow us to reach the desired state with a high enough fidelity.

The spin system is initially at equilibrium, in the thermal state; in the high-field, high-temperature limit this can be very well approximated by the state $\rho_{eq}=\Sigma_{k=1}^N\sigma_z^k$ (notice that we ignore the large component proportional to the identity since it does not evolve or contribute to the signal). By rotating the thermal equilibrium state to the transverse plane $\rho(t=0^+)=\Sigma_{k=1}^N\sigma_x^k$, the state is no longer an eigenstate of the internal Hamiltonian and will therefore evolve. This evolution is usually recorded in the NMR free induction decay (FID). It is known that the apparent decay of the magnetization masks a complex dynamics [17], where nondetectable many-body states are created from single-body magnetization terms by dipolar Hamiltonian couplings. Due to the fewer number of couplings to other spins, the first and last spins have a slower dynamics (apparent decay) at short time. (If we approximate the evolution of the polarization of each single spin by a Gaussian decay, the decay rate is $\sqrt{2}$ times smaller than for all the other spins.) It is thus possible to select a particular time t_1 at which, while the state of these two spins is still mainly σ_x, all the other spins have evolved to more complex multibody states. From the commutator expansions of the unitary evolution, we can calculate the approximate coefficients of the polarization (σ_x^k) terms for each spin as a function of time and therefore select the time at which $\sigma_x^k\approx 0$, $\forall\ k\neq 1,N$, while 44% of the polarization of the first and last spins is still conserved (since we are interested in the short-time regime, an expansion to the eighth order gives an excellent approximation). Except for very short chains (three to four spins), the polarization of all spins $k>2$ is almost equal after this very short evolution and the optimal time is nearly independent of the number of spins in the chain, therefore allowing us to choose the time t_1 even without knowing the precise (average) number of spins in a chain.

A second $\pi/2$ pulse will bring the magnetization of spins 1 and N to the longitudinal (z) axis, so that the density matrix describing the system can be written as $\rho(t_1)=\alpha(\sigma_z^1+\sigma_z^N)+\rho'$. To select only the first two terms, which are the desired state, we can recur to a phase cycling scheme that selects only terms that commute with the total magnetization along z ($\Sigma_{k=1}^N\sigma_z^k$) such as population terms. Unfortunately, we have not found a solution that also cancels out the zero-quantum terms (that is, components of the density matrix with total magnetic quantum number=0). Even with this limitation, the fidelity with the desired state is about 70% as calculated in simulations; the larger errors are given by residual polarization on spins 2 and $N-1$ as well as correlated states of the form $\sigma_z^i(\sigma_+^{i-1}\sigma_-^{i+1}+\sigma_-^{i-1}\sigma_+^{i+1})$.

III. EXPERIMENTAL SETUP

We performed experiments on a 300-MHz Bruker Avance Spectrometer, with a homebuilt probe tuned to 282.4 MHz for the observation of fluorine spins. The sample was a single crystal of fluorapatite [$Ca_5(PO_4)_3F$]. Apatites, either hydroxyapatites or fluorine-containing apatites [18,19], have been studied in NMR experiments because of their particular geometry [20,21] and have also been proposed as a system to implement QIP [22]. The fluorapatite crystallizes in the hexagonal-dipyramidal crystal system, with cell dimensions $a=9.367$ Å and $c=6.884$ Å and two formula units per cell. The fluorine spins are arranged on linear chains along the c direction, with distance between two atoms $d=3.442$ Å, and six adjacent parallel chains at the distance $D=9.367$ Å. Since the dipolar couplings decrease with the cube of the distance between spins, the spin system can be considered a quasi-1D system. In particular, by orienting the c axis of the crystal along the z direction, the ratio of the cross-chain to in-chain dipolar coupling is

$$\frac{b_\times}{b_{in}}=\frac{1}{2}\frac{d^3}{D^3}\approx 0.0248. \tag{3}$$

Although this crystal has a very good purity, as testified by long relaxation times ($T_1\sim 200$ s), the chains are interrupted by defects and vacancies, which limit their length. If we consider the short-time evolution only, the spins of different chains do not interact and behave as independent systems, while if we let the system evolve for a time long compared to the cross-chain interactions, the approximation of independent systems will fail. We will include the effects of other chains and the distribution in chain length into the environmental decoherence and only consider a single chain as the system of interest.

We applied the pulse sequence presented in the previous section:

$$\left.\frac{\pi}{2}\right|_\alpha - t_1 - \left.\frac{\pi}{2}\right|_{\bar{\alpha}}, \tag{4}$$

where the pulse axis α was phase cycled through y and x to cancel the nonzero-quantum terms. The optimal time t_1 for the dipolar coupling strength of fluorapatite (about 8 kHz for nearest-neighbor spins in chains aligned with the external magnetic field) is given by $t_1=30.5$ μs.

In order to assess qualitatively the results of this sequence, we measured a spectrum of the system, after the

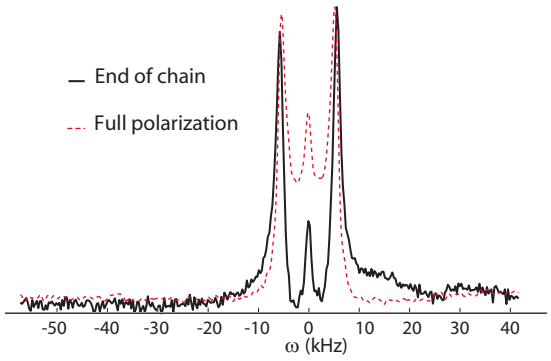

FIG. 1. (Color online) Comparison of the spectra when the polarization is retained by all spins in the chain (dashed line) and for the excitation of the extremities only (solid line). The full width at half maximum is ≈19 kHz and the distance between peaks ≈8 kHz. The experimental data were obtained with sequence (4) and a solid echo readout. The wait time t_1 was $t_1=0.5$ μs for the all-spin spectrum and 30.5 μs for the chain-end excitation. A small Teflon signal (from the tuning capacitors) can be seen in the end-of-chain signal in the 10–20 kHz region.

preparation of the desired initial state, and compared it to the thermal equilibrium spectrum (see Fig. 1). In particular, it is important to observe the state at short time, when the effects of the desired initial state should be stronger; the solid echo technique [23] was thus used, to avoid the dead time imposed by the electronics and the pulse ring-down [24]. While this kind of measurement does not give a definite answer to the question whether the polarization has been concentrated on the extremities only, the qualitative differences in the spectra measured are encouraging. In particular, we observe that resolution of the three peaks observed in the thermal state is much better (we obtain narrower lines) as expected from a state in which fewer couplings are available, and while the spectrum of the thermal state presents the characteristic of a triplet [18,19] (the ratios of the integrated peak intensities are 1:0.65:1.02) as expected for one spin coupling strongly to two equivalent spins (as is the case if we consider nearest neighbors only), the spectrum for our state is closer to a doublet (with integrated peak ratios 1:0.11:1.15), reflecting the fact that the spins at the chain extremities interact strongly with only one spin.

IV. MULTIPLE QUANTUM COHERENCE AS A STATE MEASUREMENT TOOL

Since the detection of magnetic resonance restricts the observables to the collective transverse magnetization, it is not possible to reconstruct the state of the system by quantum-state tomography [25]. To assess the efficiency of the state preparation scheme, we thus need a readout scheme that reveals the signature of the particular initial state prepared. By studying a more complex dynamics than the free induction decay, we can obtain more accurate insight into the state created. In particular, a sensitive probe of the dynamics of a correlated many-spin system is the creation and evolution of quantum coherences.

A. Fermion operator solution to MQC dynamics

Quantum coherence refers to a state of a physical system where the phase differences among the various constituents of the wave function can lead to interferences. In particular, quantum coherences often refer to a many-body system, whose parties interact and therefore show a correlation, a well-defined phase relationship. In NMR, coherences between two or more spins are usually called *multiple-quantum coherences*. When the system is quantized along the z axis, so that the Zeeman magnetic moment along z is a good quantum number, a quantum coherence of order n is defined as the transition between two states $|m_1\rangle$ and $|m_2\rangle$, such that the difference of the magnetic moment along z of these states is n: $m_1-m_2 \propto n$. Multiple-quantum coherences of order n usually describe states like $|m_2\rangle\langle m_1|$, or elements in the density matrix that correspond to a transition between these two states [26,27]. The state $|m_2\rangle\langle m_1|$ is also called a coherence of order n. Diagonal density matrix terms are called populations and do not properly describe a coherence.

The observation of multiple-quantum coherences in NMR started in the mid-1970s, as a method for unraveling complex spectra, by filtering transitions based on the coherence order involved [27]. More recently, these states have been studied with respect to their decay time and effects of decoherence on them [1,4], because of their connection to entangled states. Multiple-quantum coherences are also the basis of proposed schemes for the full characterization of complex many-spin states [28]: identifying the different coherence orders occurring in a state is the first step toward quantum-state tomography.

Coherences can be created by the interplay of rf pulses and free evolution periods, during which interactions among spins occur. Multiple-pulse sequences create Hamiltonians that can raise the coherence order of the system. One widely used sequence [8,29], for example, creates the double-quantum Hamiltonian

$$\mathcal{H}_{DQ} = \sum_{i,j} \frac{b_{ij}}{2}(\sigma_i^x\sigma_j^x - \sigma_i^y\sigma_j^y) = \sum_{i,j} b_{ij}(\sigma_i^+\sigma_j^+ + \sigma_i^-\sigma_j^-), \quad (5)$$

which raises the coherence orders in steps of 2 (thus, starting from the thermal state, only even coherence order will be created). The growth of coherence orders has been the matter of many investigations [17,30], because of its relationship to the system's geometrical structure. Because of its complexity, only stochastic models, based on the probability of occupation of different coherent states, and semiclassical models like the hopping model are available to describe this dynamics. If we restrict the evolution to one-dimensional systems, the growth of coherence is slowed down by the fewer couplings among spins; if we further assume that only nearest-neighbor couplings are present (and all equal to b), the evolution under the double-quantum Hamiltonian turns out to be exactly solvable [31,32]. Experimentally, the nearest-neighbor (NN) approximation is accurate for short times, while for longer times, weaker couplings start to produce appreciable corrections.

The most important characteristic of 1D MQC experiments are the oscillations between zero- and double-quantum

coherences at short times. It is this restriction of the accessible Hilbert space (which is exact at any time in the NN approximation) that makes the problem analytically tractable. As we will show in this section, these oscillations turn out to be a signature of the initial state, so that they can help us confirm experimentally the preparation of the initial state desired. For comparison, we derive analytically (and then measure experimentally) not only the MQC intensities for the desired state $\rho_e(0)=\sigma_z^1+\sigma_z^N$, but also for the thermal equilibrium state $\rho(0)=\Sigma_{j=1}^N\sigma_z^j$.

The analytical result is obtained by mapping the spin system to spinless fermion operators (see the Appendix):

$$c_j=-\prod_{k=1}^{j-1}(\sigma_z^k)\sigma_j^-. \tag{6}$$

The diagonalization of the double-quantum Hamiltonian [31–33] is accomplished by a Bogoliubov canonical transformation to the operators d_k [34]:

$$c_j=\frac{1}{\sqrt{N+1}}\sum_{k=1}^{N}\sin(\kappa j)(\gamma_k d_k+d_{-k}^\dagger),\quad \kappa=\frac{\pi k}{N+1}, \tag{7}$$

where $\gamma_k\equiv\mathrm{sgn}(k)$. The DQ Hamiltonian is then diagonalized to

$$\mathcal{H}_{DQ}=-2b\sum_{k=1}^{N}\cos\kappa(d_k^\dagger d_k+d_{-k}^\dagger d_{-k}-1). \tag{8}$$

We now express the two initial states in terms of Bogoliubov operators d_k. The thermal state has a particularly compact expression. Using first the spin-to-fermion mapping, we have

$$\rho(0)=\frac{1}{2}\sum_{j=1}^{N}\sigma_j^z=\sum_{j=1}^{N}\left(\frac{1}{2}-c_j^\dagger c_j\right) \tag{9a}$$

$$=\frac{N}{2}\sum_{k=1}^{N}(d_k d_{-k}-d_k^\dagger d_{-k}^\dagger), \tag{9b}$$

where in writing Eq. (9b) we used orthogonality relationships for trigonometric functions [see Eqs. (A12) and (A13) in the Appendix].

Consider now the initial state $\rho_e(0)=\frac{1}{2}(\sigma_1^z+\sigma_N^z)$. Because we are not summing over all spins, it is no longer possible to use the orthogonality relationships. This results in more cumbersome double sums

$$\rho_e(0)=\frac{1}{2}(\sigma_1^z+\sigma_N^z)=1-(c_1^\dagger c_1+c_N^\dagger c_N) \tag{10a}$$

$$=1-\frac{1}{N+1}\sum_{k,h}S_{kh}(\gamma_k d_k^\dagger+d_{-k})(\gamma_h d_h+d_{-h}^\dagger), \tag{10b}$$

where to simplify the notation we set $S_{kh}=\sin(\kappa)\sin(\eta)+\sin(N\kappa)\sin(N\eta)$.

The system evolves under the double-quantum Hamiltonian with a dynamics described by the propagator $U(t)=\exp[2ib\Sigma_k\cos\kappa(d_k^\dagger d_k+d_{-k}^\dagger d_{-k})]$. We now define the eigenphases $\psi_k=2bt\cos\kappa$. The thermal-state evolution is easily calculated to be

$$\rho(t)=\frac{1}{2}\sum_{k=1}^{N}(d_k d_{-k}e^{2i\psi_k}-d_k^\dagger d_{-k}^\dagger e^{-2i\psi_k}). \tag{11}$$

In order to separate contributions from different coherence orders, we transform back to fermion operators. To simplify the calculations, we use the operators $a_k=(\gamma_k d_k+d_{-k}^\dagger)/\sqrt{2}$, which represent the same coherence order as the c_j's operators (the d_k operators correspond instead to different coherence orders, since they are combinations of lowering and raising operators). With some algebraic manipulations, we have

$$\rho(t)=\underbrace{-\sum_k\cos\psi_k\left(a_k^\dagger a_k-\frac{1}{2}\right)}_{\rho^{(0)}}\underbrace{-\frac{i}{2}\sum_k\gamma_k\sin|\psi_k|(a_k^\dagger a_{-k}^\dagger+a_k a_{-k})}_{\rho^{(+2)}+\rho^{(-2)}}. \tag{12}$$

The intensities J_n of each nth quantum coherence as measured in the MQC experiment is given by $\mathrm{Tr}\{[U_{DQ}\rho(0)U_{DQ}^\dagger]^{(n)}(U_{DQ}\Sigma\sigma_z U_{DQ}^\dagger)^{(-n)}\}$. Notice that the contribution of population terms to the zero-quantum signal cannot be distinguished experimentally and will be therefore included in both the analytical and experimental results. Since in this case $\rho(0)=\Sigma\sigma_z$, we have $J_n=\mathrm{Tr}[\rho^{(n)}\rho^{(-n)}]$. We evaluate the trace of the fermion operators a_k and $a_k^\dagger$ in their corresponding occupational number representation, so that only terms like $a_k^\dagger a_k$ are diagonal and contribute to the trace [see Eqs. (A16) and (A17) in the Appendix]. The normalized MQC intensities for zero and double quanta are finally given by: [1]

$$J_0=\frac{1}{N}\sum_k\cos^2(4bt\cos k), \tag{13a}$$

$$J_2=\frac{1}{2N}\sum_k\sin^2(4bt\cos k). \tag{13b}$$

The evolution of the polarization on the extremities of the chain is

$$\rho_e(t)=1-\frac{1}{N+1}\sum_{k,h=1}^{N}S_{kh}(d_k^\dagger e^{-i\psi_k}+d_{-k}e^{i\psi_k})\times(d_h e^{i\psi_h}+d_{-h}^\dagger e^{-i\psi_h}). \tag{14}$$

Again, we transform to fermion operators to distinguish contributions from different coherence orders:

[1] Notice the discrepancy with the result in [31] which is due to incorrect boundary conditions. We confirmed our results with numerical calculations for short chains.

$$\rho_e(t) = \underbrace{\frac{i}{2}\frac{1}{N+1}\sum_{k,h} S_{kh}\sin(\psi_k+\psi_h)(a_h^\dagger a_{-k}^\dagger - a_{-k}a_h)}_{\rho^{(+2)}+\rho^{(-2)}}$$

$$\underbrace{+1-\frac{1}{N+1}\sum_{k,h} S_{kh}[a_k^\dagger a_h\cos(\psi_k+\psi_h)+\delta_{k,h}\sin\psi_k^2]}_{\rho^{(0)}}. \quad (15)$$

As expected, also starting from the noncollective initial state only zero- and double-quantum coherences are developed (taking into account nearest-neighbor couplings only).

The zero-quantum contribution to the signal is $J_0^e = \mathrm{Tr}[\rho_e^{(0)}\rho^{(0)}]$ [with $\rho^{(0)}(t)$ from Eq. (12)]:

$$J_0^e = -\sum_k \cos\psi_k \mathrm{Tr}\left[a_k^\dagger a_k - \frac{1}{2}\right] + \frac{1}{(N+1)}\sum_{k,h,l} S_{kh}\cos\psi_l\cos(\psi_k+\psi_h)\mathrm{Tr}[a_k^\dagger a_h a_l^\dagger a_l] + \frac{1}{(N+1)}\sum_{k,l} S_{kk}\cos\psi_l\sin\psi_k^2\,\mathrm{Tr}\left[a_k^\dagger a_k - \frac{1}{2}\right]. \quad (16)$$

Using the trace and trigonometric identities in the Appendix, we find the normalized zero-quantum intensity

$$J_0^e = \frac{2}{(N+1)}\sum_k \sin^2(\kappa)\cos^2(4bt\cos\kappa). \quad (17)$$

The double-quantum intensity J_2^e is given by

$$J_2^e = \mathrm{Tr}[\rho_e^{(2)}\rho^{(-2)}] = \frac{1}{(N+1)}\sum_{k,h,l} S_{kh}\sin\psi_l \times \frac{1}{2}\sin(\psi_k+\psi_h)\mathrm{Tr}[a_h^\dagger a_{-k}^\dagger a_l a_{-l}], \quad (18)$$

which yields

$$J_2^e = \frac{1}{(N+1)}\sum_k \sin^2(\kappa)\sin^2(4bt\cos\kappa). \quad (19)$$

These more complex expressions lead to a very different behavior of the coherence intensities as shown in Fig. 2, so that it is possible to distinguish even experimentally what the initial condition of the system was.

B. Experimental results

We applied the pulse sequence (4) followed by a MQC-experiment sequence. In particular, we used the 16-pulse sequence [29] (except for the three shorter time values, where the 8-pulse sequence was used [8]) and a phase cycling with increments of $\varphi = 2\pi/8$ to select up to the fourth coherence order, by repeating the experiment 16 times.

The time delay between pulses in the MQC sequence was varied from 2 to 6.5 μs, to increase the excitation time, as well as the number of repetitions of the sequence itself (one or two loops), so that the evolution of the quantum coherences were studied between the times of 37.6 and 354.4 μs.

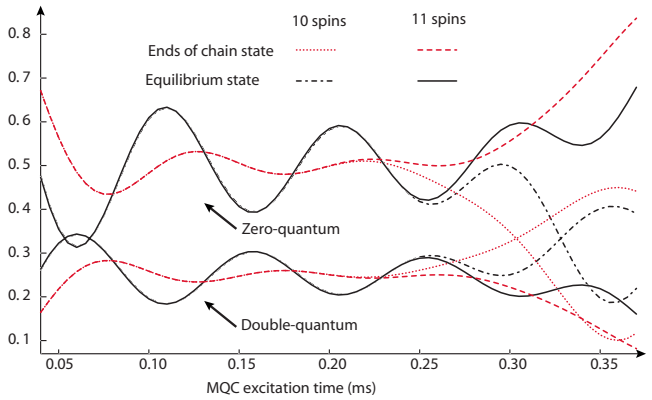

FIG. 2. (Color online) Zero- and double-quantum intensities as a function of the evolution time under the double-quantum Hamiltonian. Nearest-neighbor couplings only are assumed, with equal strength as given by the fitting to experimental data (see Fig. 3). In particular notice the clear differences in the behavior for the two initial states. Also the even-odd spin number dependence of the MQC intensities is interesting: while this tends to go to zero for large number of spins in the collective initial-state case, this difference is observed even for very large number of spins for the other initial state.

We compare the results obtained with the evolution for the thermal equilibrium as initial state. In order to take into account the effects of imperfections in the pulse sequence, we applied the pulse sequence as in (4) also to obtain the thermal state, with a very short t_1 time ($t_1 = 0.5$ μs). In Fig. 3 we show the dynamics of the zero- and double-quantum intensities, normalized to have sum=1 to take into account the signal decay for longer excitation times. We notice that the four-quantum coherence intensity is not distinguishable from the noise, indicating that the time scale is short enough for the nearest-neighbor approximation to be valid to a good extent (remember that the NN approximation predicts that only zero- and double-quantum coherences are excited).

The experimental results for the MQC oscillations starting from the thermal state have been fitted to the theoretical curve (13) for a single chain with nearest-neighbor couplings only. The dipolar strength and the number of spins were the fitting parameters. The results of this fitting were used to plot the theoretical curve for the chain-end initial state [Eqs. (17) and (19)]. The concordance of the theoretical predictions with the experimental data is very good, even if the state created contains residual zero-quantum terms.

The best fitting of the experimental data in Fig. 3 to (13) was found for a chain length of 11 spins. This result must be taken with caution, since the chain length influences only the long-time behavior of the MQC intensities, where other factors not taken into account in the simple analytical model start to play an important role. In particular, the experimental results for the chain ends indicate that there are either longer chains or a distribution of short chains, with an odd and even number of spins. Although the reason for the best fit at 11 spins could be simply due to a distribution of spin chains around a mean of 11 spins, the low impurity content of the crystal studied is not in agreement with this finding. We believe that a more plausible reason is the breakdown of the

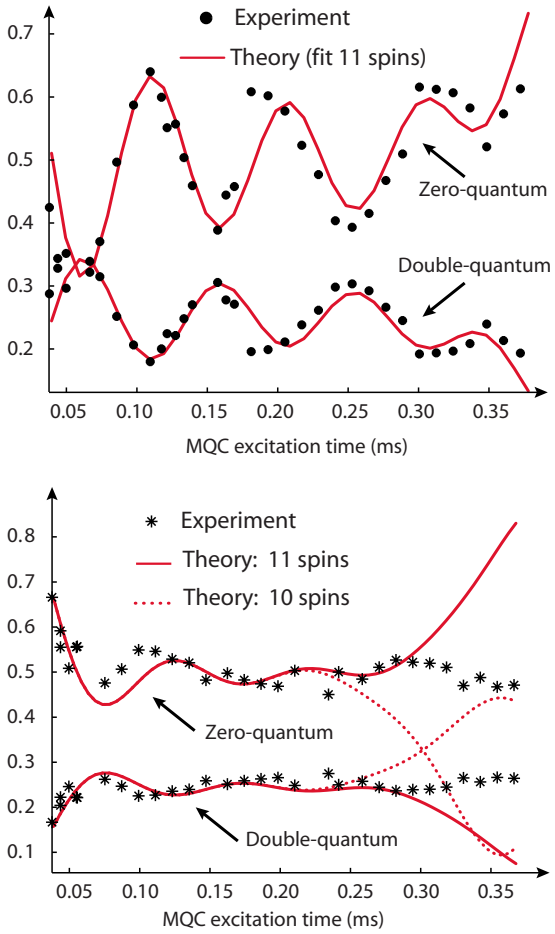

FIG. 3. (Color online) Experimental results. Top: the initial state is the collective thermal state $\Sigma_k \sigma_z^k$. The experimental points have been fitted (solid line) to the theoretical curves for nearest-neighbor coupling only, with the dipolar coupling as fitting parameter. The number of spins was varied to find the best fit, which results in being $N=11$ spins. Bottom: MQC intensities for the initial state $\rho_0=\sigma_z^1+\sigma_z^N$. Also plotted are the theory predictions for the same dipolar coupling and 11 spins (solid line) or 10 spins (dotted line). The experimental behavior observed (a constant behavior also for longer time) indicates that a simple model with 11 spin chains is not an accurate description at longer times (see text).

model of isolated nearest-neighbor coupled spin chains. Even if next-nearest-neighbor couplings and couplings to adjacent chains are not strong enough yet to create four-quantum coherences, they still modify the intensities of the zero- and double-quantum coherences. Further experiments would be needed to distinguish between these hypotheses.

V. CONCLUSIONS

We have studied a naturally occurring physical system, a single crystal of FAp that presents linear chains of spin-1/2 particles. Since the physical characteristics of the system and the experimental apparatus do not provide universal control of the quantum spin system, we propose to use this system not as a candidate quantum computer, but as a specific task-oriented QIP device—for example, for quantum-state transport or simulations. In particular, we have devised a scheme, combining unitary and nonunitary control, for creating a particular state that breaks the natural symmetry of the system. This state will allow us to study properties of state transport along the chain as well as being an interesting initial state for simulations. Furthermore, preparation of this state is a first step toward universal control of the system, since full control of the spins at the chain ends (in addition to collective control over all other spins) ensures universality.

In addition, we have investigated a tool for acquiring a deeper knowledge of the state and dynamics of the system, given the limitations in the readout procedures. Multiple-quantum coherences allow us to gather more information on the multibody aspects of the system than simple direct observation of the collective polarization. In particular, we used analytical solutions in the limit of nearest-neighbor couplings to interpret the experimental results which confirm the preparation of the desired state.

In conclusion, we have shown how even a quantum system without universal control can be used to study physical problems of interest in condensed-matter theory and quantum-information science.

ACKNOWLEDGMENTS

This work was supported in part by the National Security Agency (NSA) under Army Research Office (ARO) Contracts Nos. DAAD190310125 and W911NF-05-1-0459, by DARPA, and by the National Science Foundation under Grant No. 0403809, and through a grant for the Institute for Theoretical Atomic, Molecular and Optical Physics at Harvard University and Smithsonian Astrophysical Observatory. We thank T. Ladd for providing us the fluorapatite crystal.

APPENDIX: FERMION OPERATORS

Spin operators of the Pauli group can be mapped to fermion operators, obeying the well-known anticommutation relationships. This mapping is useful in describing the dynamics of various 1D models, since some Hamiltonians can then be diagonalized analytically. In the following we describe a particular mapping that is suited for describing the creation of MQC.

A mapping from spin to fermion operators goes back to Jordan and Wigner [35], who first transformed quantum spin $S=1/2$ operators, which commute at different lattice sites, into operators obeying a Clifford algebra (fermions). This transformation was used to map the one-dimensional Ising model onto a spinless fermion model, which is exactly solvable. The Jordan-Wigner transformation has been recently generalized to the cases of arbitrary spin S [36,37] and to 2D spin systems [38].

Given a set of spin-$\frac{1}{2}$ operators σ_j^α, each defined at a lattice site j, they obey the commutation relationship

$$[\sigma_j^\alpha, \sigma_k^\beta] = \delta_{j,k} i \sigma_j^\gamma, \tag{A1}$$

where $\{\alpha,\beta,\gamma\}=\{x,y,z\}$ and cyclic permutations of these indices. The raising and lowering operators $\sigma_j^\pm=(\sigma_j^x \pm i\sigma_j^y)/2$ obey mixed commutation and anticommutation relationships,

which are not preserved under a unitary transformation. To diagonalize the spin Hamiltonian we must thus use the Jordan-Wigner transformations to map these operators onto fermion operators c_j and $c_j^\dagger$, obeying the canonical anticommutation relationships

$$\{c_j^\dagger, c_k\} = \delta_{j,k}, \quad \{c_j, c_k\} = \{c_j^\dagger, c_k^\dagger\} = 0, \tag{A2}$$

where we adopted the notation $\{\cdot,\cdot\}$ for anticommutators. A basis for the Hilbert space of these operators is given by the occupation number representation $|n\rangle = |n_1, n_2, \ldots, n_N\rangle$, where $n_j = \{0,1\}$ is the occupation number at site j. The state $|n\rangle$ can be obtained from the vacuum state by

$$|n\rangle \equiv \prod_j (c_j^\dagger)^{n_j} |\text{vac}\rangle. \tag{A3}$$

Then, the action of the fermion operators on such states is given by

$$c_j|n\rangle = \begin{cases} 0, & \text{if } n_j = 0, \\ -(-1)^{s_j^n}|n'\rangle, & \text{otherwise}, \end{cases} \tag{A4}$$

where $|n'\rangle$ is the vector resulting when the jth entry of $|n\rangle$ is changed to 0 and $s_j^n = \Sigma_{k=1}^{j-1} n_k$. Analogously,

$$c_j^\dagger|n\rangle = \begin{cases} 0, & \text{if } n_j = 1, \\ -(-1)^{s_j^n}|n'\rangle, & \text{otherwise}, \end{cases} \tag{A5}$$

where $|n'\rangle$ is the vector resulting when the jth entry of $|n\rangle$ is changed to 1.

The mapping from spin to fermion operators can be expressed in several ways, the most intuitive being based on identifying every basis vector $|n\rangle$ in the occupation number representation basis to the corresponding $|n\rangle$ basis vector in the computational basis for the spin operator Hilbert space. Imposing this one-to-one correspondence on basis states and taking into account the respective actions of spin and fermion operators on their basis vectors, one obtains the mapping

$$c_j = -\prod_{k=1}^{j-1} \sigma_k^z \sigma_j^-, \quad \sigma_j^- = -\prod_{k=1}^{j-1} (1 - 2c_k^\dagger c_k) c_j,$$

$$c_j^\dagger = -\prod_{k=1}^{j-1} \sigma_k^z \sigma_j^+, \quad \sigma_j^+ = -\prod_{k=1}^{j-1} (1 - 2c_k^\dagger c_k) c_j^\dagger. \tag{A6}$$

Notice also that $\sigma_j^z = 1 - 2c_j^\dagger c_j$.

Consider now the double-quantum Hamiltonian with equal couplings restricted to the nearest-neighbor spins:

$$\mathcal{H}_{DQ} = b \sum_{j=1}^{N} \sigma_j^+ \sigma_{j+1}^+ + \sigma_j^- \sigma_{j+1}^-. \tag{A7}$$

We can express it in terms of the fermion operators as

$$\mathcal{H}_{DQ} = b \sum_{j=1}^{N} \prod_{l=1}^{j} (1 - 2c_l^\dagger c_l) c_{j+1}^\dagger \prod_{l=1}^{j-1} (1 - 2c_l^\dagger c_l) c_j^\dagger + \text{H.c.}$$

$$= -b \sum_{j=1}^{N} c_{j+1}^\dagger c_j^\dagger + c_j c_{j+1} = C^\dagger \hat{B} C, \tag{A8}$$

where we introduced the vector $C^\dagger = [c^\dagger c]$ and the matrix $\hat{B}$:

$$\hat{B} = \begin{bmatrix} 0 & B \\ -B & 0 \end{bmatrix}, \quad B = -b(\delta_{i,j+1} - \delta_{i,j-1}). \tag{A9}$$

Notice that even if the mapping to fermion operators is nonlocal, this quadratic Hamiltonian is mapped onto a local Hamiltonian when one considers only nearest-neighbor couplings. The matrix $\hat{B}$ is orthogonal and can therefore be put into diagonal form, with eigenvalues $\cos(\frac{\pi k}{N+1})$, $k = 1, 2, \ldots, N$, and eigenvectors $D^\dagger = [d^\dagger d]$. The diagonalization is a canonical unitary (orthogonal) transformation (a Bogoliubov transformation) to a diagonal basis satisfying the same anticommutation relationships [33]. To simplify the diagonalization we need to introduce also the negative modes operators d_k and correspondingly the fermion operators c_j (with $j < 0$), by extending the sum in (A8) from $-N$ to N.

We can express the fermion operators c_j in terms of the Bogoliubov operators d_k by the following orthogonal relationship:

$$c_j = \frac{1}{\sqrt{N+1}} \sum_{k=1}^{N} \sin(\kappa j)(\gamma_k d_k + d_{-k}^\dagger), \quad \kappa = \frac{\pi k}{N+1}, \tag{A10}$$

where $\gamma_k = \text{sgn}(k)$, ensuring the transformation is orthogonal (this transformation is obtained by imposing the condition that the resulting DQ Hamiltonian be diagonal). Substituting expression (A10) into Eq. (A8) we have

$$\mathcal{H}_{DQ} = -b \sum_{k,h=1}^{N} [(\gamma_k d_k + d_{-k}^\dagger)(\gamma_h d_h + d_{-h}^\dagger) + \text{H.c.}]$$

$$\times \frac{1}{N+1} \sum_{j=-N}^{N} \sin(\kappa j) \sin[\eta(j+1)] \tag{A11}$$

[with $\eta = \pi h/(N+1)$]. By using the orthogonality relationships

$$\frac{1}{N+1} \sum_{j=-N}^{N} \sin(kj)\sin(hj) = (\delta_{k,h} - \delta_{k,-h}) \tag{A12}$$

and

$$\sum_{j=-N}^{N} \sin(kj)\cos(hj) = 0, \tag{A13}$$

we can simplify the Hamiltonian (A11):

$$\mathcal{H}_{DQ} = -2b\sum_{k=1}^{N} \cos\kappa(d_k^\dagger d_k + d_{-k}^\dagger d_{-k} - 1). \quad \text{(A14)}$$

We note that under this diagonal Hamiltonian, the operators d_k evolve as $d_k(t) = e^{-i\mathcal{H}_{DQ}t} d_k e^{i\mathcal{H}_{DQ}t} = e^{-2ib\cos\kappa} d_k$.

For convenience, we introduce also fermion operators a_k, which are useful in expressing the density matrix:

$$a_k = (\gamma_k d_k + d_{-k}^\dagger)/\sqrt{2}. \quad \text{(A15)}$$

The following identities for the trace of fermion operators have been used in the text to calculate the zero- and double-quantum intensities:

$$\mathrm{Tr}[a_k^\dagger a_k] = 2^{N-1},$$

$$\mathrm{Tr}[a_h^\dagger a_h a_{k'}^\dagger a_{k'}] = \begin{cases} 2^{N-2} & \text{for } k \neq k', \\ 2^{N-1} & \text{for } k = k', \end{cases} \quad \text{(A16)}$$

$$\mathrm{Tr}[a_h^\dagger a_{-k}^\dagger a_{-k'} a_{h'}] = \begin{cases} 2^{N-2} & \text{for } k = k', h = h', \\ -2^{N-2} & \text{for } k = -h', h = -k', \\ 0 & \text{otherwise.} \end{cases} \quad \text{(A17)}$$

[1] H. G. Krojanski and D. Suter, Phys. Rev. Lett. **93**, 090501 (2004).
[2] A. Fedorov and L. Fedichkin, J. Phys.: Condens. Matter **18**, 3217 (2006).
[3] J. Schliemann, A. V. Khaetskii, and D. Loss, Phys. Rev. B **66**, 245303 (2002).
[4] H. J. Cho, P. Cappellaro, D. G. Cory, and C. Ramanathan, Phys. Rev. B **74**, 224434 (2006).
[5] D. Burgarth, V. Giovannetti, and S. Bose, J. Phys. A **38**, 6793 (2005).
[6] J. Fitzsimons and J. Twamley, Phys. Rev. Lett. **97**, 090502 (2006).
[7] Joseph Fitzsimons, Li Xiao, Simon C. Benjamin, and Jonathan A. Jones, Phys. Rev. Lett. **99**, 030501 (2007).
[8] J. Baum, M. Munowitz, A. N. Garroway, and A. Pines, J. Chem. Phys. **83**, 2015 (1985).
[9] D. Burgarth and S. Bose, Phys. Rev. A **71**, 052315 (2005).
[10] M. Paternostro, G. M. Palma, M. S. Kim, and G. Falci, Phys. Rev. A **71**, 042311 (2005).
[11] S. Bose, Phys. Rev. Lett. **91**, 207901 (2003).
[12] A. Kay, Phys. Rev. Lett. **98**, 010501 (2007).
[13] D. Burgarth, V. Giovannetti, and S. Bose, Phys. Rev. A **75**, 062327 (2007).
[14] D. Jaksch and P. Zoller, Ann. Phys. (N.Y.) **315**, 52 (2005).
[15] P. Cappellaro, C. Ramanathan, and D. Cory, e-print arXiv:quant-ph/0706.0342.
[16] R. Romano and D. D'Alessandro, Phys. Rev. A **73**, 022323 (2006).
[17] H. J. Cho, T. D. Ladd, J. Baugh, D. G. Cory, and C. Ramanathan, Phys. Rev. B **72**, 054427 (2005).
[18] M. Engelsberg, I. J. Lowe, and J. L. Carolan, Phys. Rev. B **7**, 924 (1973).
[19] W. V. der Lugt and J. Caspers, Physica (Amsterdam) **30**, 1658 (1964).
[20] G. Cho and J. P. Yesinowski, Chem. Phys. Lett. **205**, 1 (1993).
[21] G. Cho and J. P. Yesinowski, J. Phys. Chem. **100**, 15716 (1996).
[22] T. D. Ladd, J. R. Goldman, A. Dana, F. Yamaguchi, and Y. Yamamoto, e-print arXiv:quant-ph/0009122.
[23] W.-K. Rhim, A. Pines, and J. S. Waugh, Phys. Rev. Lett. **25**, 218 (1970).
[24] E. Fukushima and S. B. W. Roeder, *Experimental Pulse NMR: A Nuts and Bolts Approach* (Addison-Wesley, Reading, MA, 1981).
[25] D. T. Smithey, M. Beck, M. G. Raymer, and A. Faridani, Phys. Rev. Lett. **70**, 1244 (1993).
[26] S. Vega and A. Pines, J. Chem. Phys. **66**, 5624 (1977).
[27] M. Munowitz and A. Pines, Adv. Chem. Phys. **66**, 1 (1987).
[28] J. D. van Beek, M. Carravetta, G. C. Antonioli, and M. H. Levitt, J. Chem. Phys. **122**, 244510 (2005).
[29] C. Ramanathan, H. Cho, P. Cappellaro, G. S. Boutis, and D. G. Cory, Chem. Phys. Lett. **369**, 311 (2003).
[30] M. Munowitz, A. Pines, and M. Mehring, J. Chem. Phys. **86**, 3172 (1987).
[31] E. B. Fel'dman and S. Lacelle, J. Chem. Phys. **107**, 7067 (1997).
[32] S. I. Doronin, I. I. Maksimov, and E. B. Fel'dman, JETP **92**, 597 (2000).
[33] E. Lieb, T. Schultz, and D. Mattis, Ann. Phys. (N.Y.) **16**, 407 (1961).
[34] D. C. Mattis, *The Theory of Magnetism* (Springer-Verlag, New York, 1985).
[35] P. Jordan and E. Wigner, Z. Phys. **47**, 631 (1928).
[36] C. D. Batista and G. Ortiz, Phys. Rev. Lett. **86**, 1082 (2001).
[37] A. Anfossi and A. Montorsi, J. Phys. A **38**, 4519 (2005).
[38] F. Verstraete and J. I. Cirac, J. Stat. Mech.: Theory Exp. 2005, P09012.